Hydraulic Fracture Propagation in a Multi-Layer Fractured Media*

Leonardo Cruz[1], Ghazal Izadi[2], Colleen Barton[2], and Tobias Hoeink[3]

Search and Discovery Article #42201 (2018)**
Posted April 30, 2018

*Adapted from extended abstract prepared in conjunction with oral presentation given at the GEO 2018 13th Middle East Geosciences Conference and Exhibition, Manama, Bahrain, March 5-8, 2018

[1]Baker Hughes, Palo Alto, CA, United States (leonardo.cruz@bakerhughes.com)
[2]Baker Hughes, Palo Alto, CA, United States
[3]Baker Hughes, Houston, TX, United States

Abstract

This study explores the role of natural fractures for hydraulic fracture propagation, quantifies its effect on fracture geometry, and identifies conditions that promote an effective stimulation, using a 3D fully-coupled finite-element simulator. Several models of hydraulic fracture growth are executed in a multi-layer formation containing layers of variable stress, elastic properties, and fracture toughness, while parameters such as the coefficient of fault friction, stress contrast, fracture intersection angle, and fluid viscosity are systematically varied. Results indicate that the presence of natural fractures has a considerable effect on hydraulic fracture geometry. Compared to a reference case without natural fractures, cases with natural fractures show reduced fracture length and average width, and increased height and maximum width, except for a case with 60° fracture-intersection angle dipping 90°, in which the fracture height was reduced but its average width increased. A relative reduction in the friction coefficient generated an overall hydraulic fracture width reduction, and a relative increase in the stress contrast generated a hydraulic fracture height increase. The effective fracture area can be maximized when conditions are suitable for proppant to enter natural fractures; these conditions can be realized by selecting an optimum combination of proppant size and fluid viscosity.

Introduction

Unconventional oil and gas reservoirs contain rock discontinuities such as faults and natural fractures that have the potential to control how a hydraulic fracture grows and interacts with the rock formations during fracture stimulation operations. These discontinuities play a significant role during fracture stimulation and are fundamental to enhance primary and secondary oil/gas recovery (Carlson and Mercer, 1991). Geologic evidence and mine-back experiments show that, in places where mechanically layered rock exist, the interaction between hydraulic fractures (natural or induced) and geologic interfaces can be very complex (Warpinski et al., 1982). Natural fractures and faults, when intersected by a hydraulic fracture, can be activated by opening and/or slipping processes, diverting injection fluid into them, and increasing their fluid pressure and aperture (width). Alternatively, a natural fracture can be crossed by a hydraulic fracture with little or no fluid intake. Stress perturbations

could lead to reactivation of other optimally-oriented discontinuity planes, even in cases where they remain sealed or closed. In cases where shear displacement occurs, permeability could be enhanced (Johri and Zoback, 2013), even in planes where proppant is not present.

The hydraulic fracture propagation process in the presence of a heterogeneous and discontinuous medium is an essentially complex process, and how fractures react to realistic variations in the media is an evolving research subject that has been traditionally tackled using 2D simulators. More recently this topic has been addressed using complex 3D hydraulic fracture modeling tools with encouraging results (Izadi et al., 2015; Cruz et al., 2016; Cruz et al., 2017). In this study we attempt to quantify the first order effect of natural fracture geometry, properties, and material layering, on hydraulic stimulation geometry (e.g., fracture containment, fracture dimension, and proppant placement) using recent advances in 3D modeling.

Methodology

In this study, a fully-coupled 3D hydraulic fracturing simulator is used to systematically evaluate the role of geological discontinuities, specifically joints/natural fractures, and in situ stress and mechanical contrasts in hydraulic fracture propagation. In these models, a single vertical fracture is hydraulically propagated in a multilayered (Table 1) and discontinuous medium (Figure 1 and Figure 2) that include layers with different stress magnitudes (e.g., minimum and maximum horizontal stress) and mechanical properties (e.g., Young's modulus [E], Poisson's ratio [v], and fracture toughness [KIc]). Two symmetric and vertical natural fractures were centered in the middle layer at 150 ft. from the perforation point at opposite sides from the injection point to study how stresses and geometries changed in and around the fractures. Multiple runs, varying the natural fracture angle, friction coefficient, stress contrast, and the presence of proppant (Table 2), were included and analyzed to complete a parametric study.

The stimulation fluid was injected into the perforation at a rate of 20 bbl./min for 20 min, including 10 min of a clean fluid (viscosity =1 cP; and density = 1 kg/m^3), and 10 min of a slurry (proppant density = 2643 kg/m^3; proppant loading = 0.2396 kg/l; US-mesh size = 40/70), when proppant was considered, otherwise clean fluid was used during the 20 min pumping time. This software includes several integrated numerical methods that enable coupling different solvers such as finite element method (FEM), finite volume method (FVM), and discrete displacement method (DDM). This platform fully captures the three-dimensional hydraulically-driven fracture propagation processes by explicitly coupling the FVM that handles the flow along the fractures that are created in the faces of the solid mesh. It uses a stress intensity factor-based criterion based on linear elastic fracture mechanics (LEFM).

Results

The hydraulic fractures propagated vertically and parallel to the maximum horizontal stress (SHmax) and perpendicular to the minimum horizontal stress (Shmin), in the predefined normal stress regime, where the overburden (Sv) is the largest principal stress (Sv > SHmax > Shmin). The hydraulic fractures are mostly contained within the middle layer with some incursions toward the upper layer. The largest fracture length (Figure 3) and smallest fracture height (Figure 4) were observed in the base case without natural fractures (BaseNoFractures). The smallest fracture length and largest fracture height were observed in the model with 1000 psi (Base1000psi) stress contrast. All other modeled fracture lengths and heights were contained within this envelop, including the 60°-natural-fracture case (Base60), which length was within

average but its height plot toward the lower envelop boundary (Orange line in Figure 4). The largest fracture width (Figure 5) developed in the Base60 case, and the smallest width was observed in the BaseNoFractures model. All other modeled fracture widths were more or less contained within this envelop. The fracture width in the model with reduced friction coefficient (BaseMu03) experienced a considerable reduction starting at ~ 9 min of pumping, which occurs earlier than reductions observed in any other model.

The distribution of Shmin, in a vertical plane perpendicular to the center of the hydraulic fractures, is shown in Figure 6. The fluid injection generated an increase in Shmin, creating a stress shadow around the stimulated fracture. This perturbation had an oval shape and, in all cases, penetrated the upper and lower layers, increasing Shmin in average ~ 1 MPa around the fracture faces. The distribution of SHmax in a horizontal plane through the center of the perforation is shown in Figure 7. The stimulation generated an increase in the SHmax, forming an oval halo around the hydraulic fracture, but much smaller than the stress magnitude change observed in Shmin. This perturbation was in average ~ 0.1 MPa, but with strong stress concentration at the tips of the natural fractures.

One model (BaseProppant) included proppant injection (Figure 8) according to the schedule described in the methodology. In this case, the hydraulic fracture initially propagated similar to the other models, but the onset of proppant, which effectively increases the viscosity, generated an increase in the fracture width (Figure 5). The pumped proppant was unable to intersect the natural fractures, thus it accumulated by the natural fractures and also at the bottom of the stimulated fracture. Subsequently, the proppant bypassed the natural fractures at the bottom, but it never leaked off into the natural fractures or propped them open.

Discussion

In all modeled cases, the natural fractures acted as fluid barriers and affected fracture geometry in different ways. This can be clearly seen in the aperture plot in Figure 9, which shows the relative aperture increase between the two natural fractures except for the BaseNoFractures case where the aperture distribution is very smooth. Since the pumped fluid volume is the same across all cases and the natural fractures and stress layers acted as effective barriers accumulating fluid in the central part of the models, the hydraulic fracture in the BaseNoFracture case is longer and shorter compared to the other modeled cases.

In all natural fracture cases, the increase in fluid volume between the naturals fractures led to stress increase that generated penetration of the hydraulic fracture into the upper layer, which had the smallest fracture toughness among the three layers and may have facilitated the upper incursions. This process led to a relative increase in fracture height in all models when compared to the BaseNoFracture case. This effect was less prominent in the Base60 case where the stress perturbation was not ideal for upward fracture propagation.

In the BaseMu03 case, the observed reduction in friction coefficient may have led to enhanced slip on the natural fracture plane, which allowed stresses to dissipate, reducing the relative hydraulic fracture width. The friction coefficient is often an assumed parameter in modeling since data to effectively quantify it is usually scarce, but its relevance in hydraulic fracture modeling is obvious as shown by these models. Maximizing the fracture width is one of the main objectives of hydraulic fracture stimulation by optimizing the proppant placement, but a reduced fracture width negatively affects proppant distribution and production.

The stress contrast between the layers, often assumed one of the controlling parameters of hydraulic fracture propagation, generated a somewhat small effect in the final fracture geometry for the stress ranges (300-1000 psi) tested in these models. The variations in the stress contrast with respect to the base case, led to an increase in fracture height, the most prominent was observed in the base 1000 psi case, at the expense of a decrease in fracture width.

The Base60 case, provided the natural fracture angle that generated the largest hydraulic fracture width, which could be considered the best candidate for effective proppant placement, although proppant never entered the natural fractures. The role of natural fractures in stimulation is still a subject of debate but its effect cannot be overlook and must be considered during stimulation operations and for optimization and design.

Conclusions

- Presence of natural fractures reduced the length and increased the height and maximum width of the hydraulic fracture when compared to a reference case without natural fractures
- A reduction in the friction coefficient, generated an overall maximum width reduction in the hydraulic fracture
- An increase in the stress contrast, generated a fracture height increase in the hydraulic fracture
- 60-degree natural fractures, reduced the hydraulic fracture height but increased the maximum and average hydraulic fracture width
- An increase in the apparent viscosity (proppant case), generated a fracture width increase, similar to the 60-degree natural fracture case. Although proppant, did not enter the natural fractures, fluid viscosity is one of the engineering parameters that can be used to optimize fracture design.

References Cited

Carlson, E.S., and J.C. Mercer, 1991, Devonian Shale Gas Production: Mechanisms and Simple Models: Journal of Petroleum Technology, v. 43/04), p. 476-482.

Cruz, L., P. Fu, G. Izadi, D. Moos, J. Sheridan, R.R. Settgast, and F.J. Ryerson, 2016, The Role of Natural Fractures (Joints) in the Marcellus Shale during Hydraulic Fracture Stimulation Using Full 3D Modeling: Unconventional Resources Technology Conference (URTEC), URTec 2447719, 14 p.

Cruz, L., L. Chiaramonte, M. Gaither, G. Izadi, and D. Moos, 2017, Influence of Faults and Natural Fractures on Fracture Stimulation in the Vaca Muerta Formation Using Full 3D Modeling: 51st US Rock Mechanics/Geomechanics Symposium, American Rock Mechanics Association, ARMA 17-1006, 7 p.

Izadi, G., M. Gaither, L. Cruz, C. Baba, D. Moos, and P. Fu, 2015, Fully 3D Hydraulic Fracturing Model: Optimizing Sequence Fracture Stimulation in Horizontal Wells: 49th US Rock Mechanics/Geomechanics Symposium, American Rock Mechanics Association, ARMA-2015-119, 8 p.

Johri, M., and M.D. Zoback, 2013, The Evolution of Stimulated Reservoir Volume during Hydraulic Stimulation of Shale Gas Formations: Paper SPE presented at the Unconventional Resources Technology Conference, Denver, Colorado, USA, 12-14 August, URTec 1575434, 11 p.

Warpinski, N.R., R.A. Schmidt, and D.A. Northrop, 1982, In-situ Stresses: The Predominant influence on Hydraulic Fracture Containment: Journal of Petroleum Technology, v. 34/03, p. 653-664.

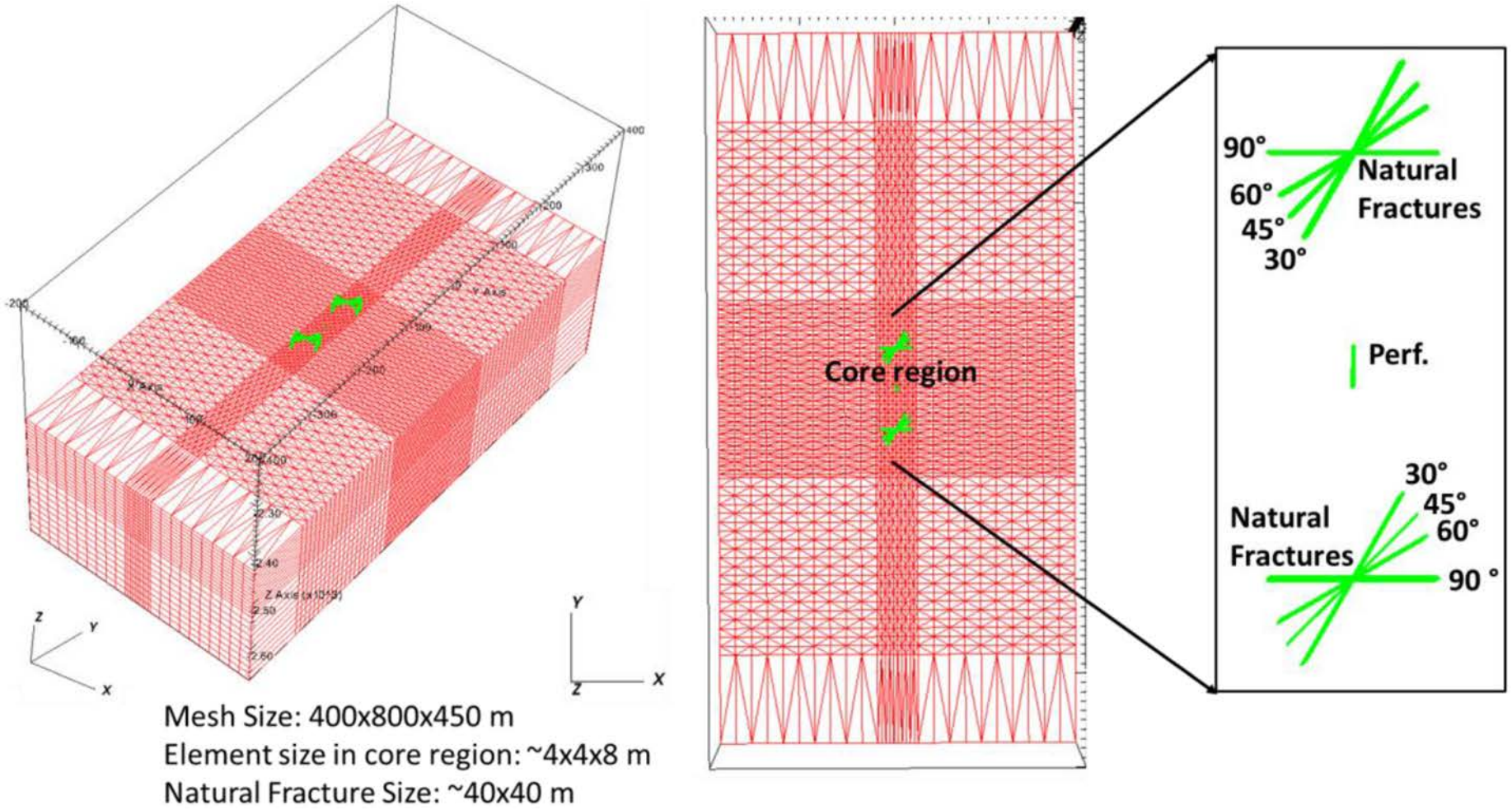

Figure 1. Oblique and map view of mesh, and geometry of natural fractures included in the multilayered stimulation study.

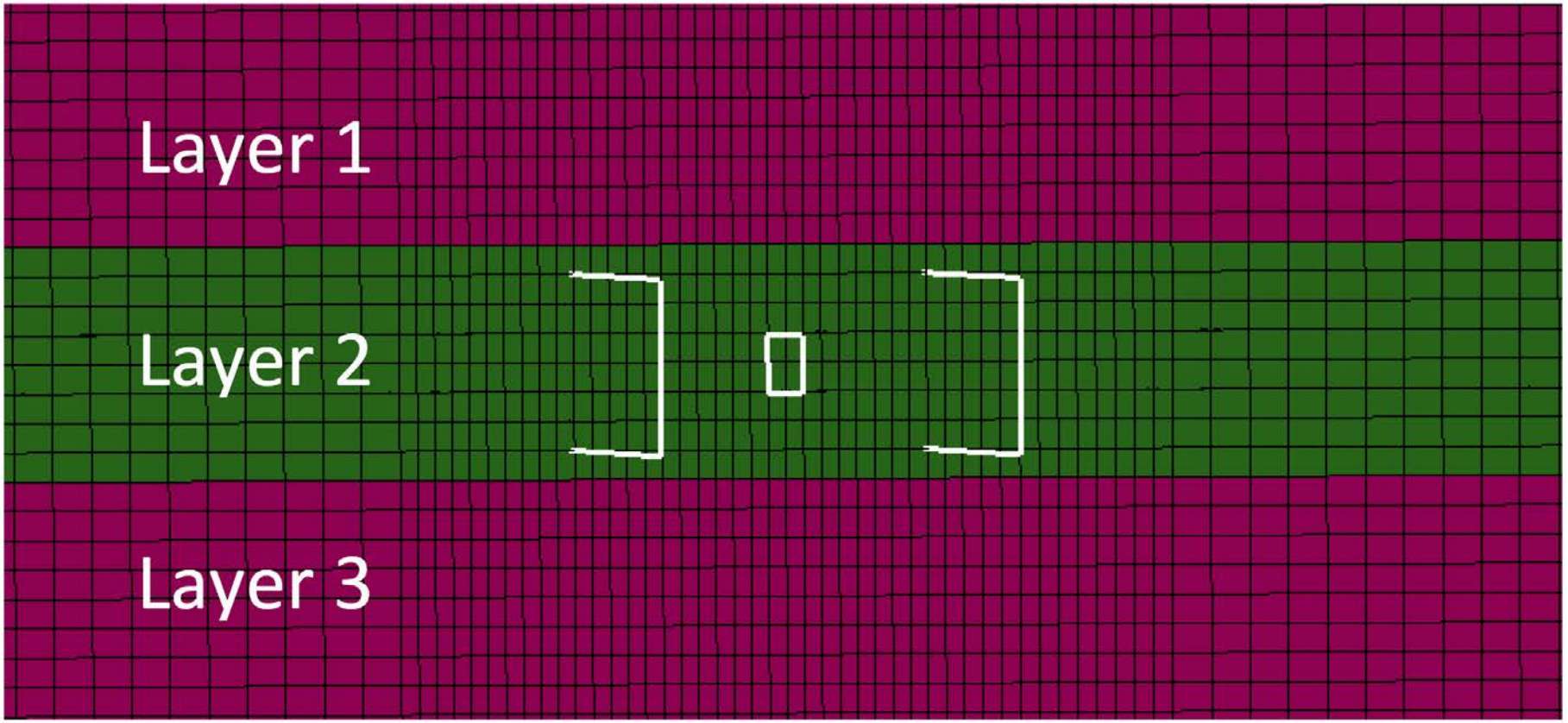

Figure 2. Cross-section view of mesh (black lines) and geometry of natural fractures and perforation (white lines) of the base case (45° fractures). The section is parallel to hydraulic fracture propagation direction.

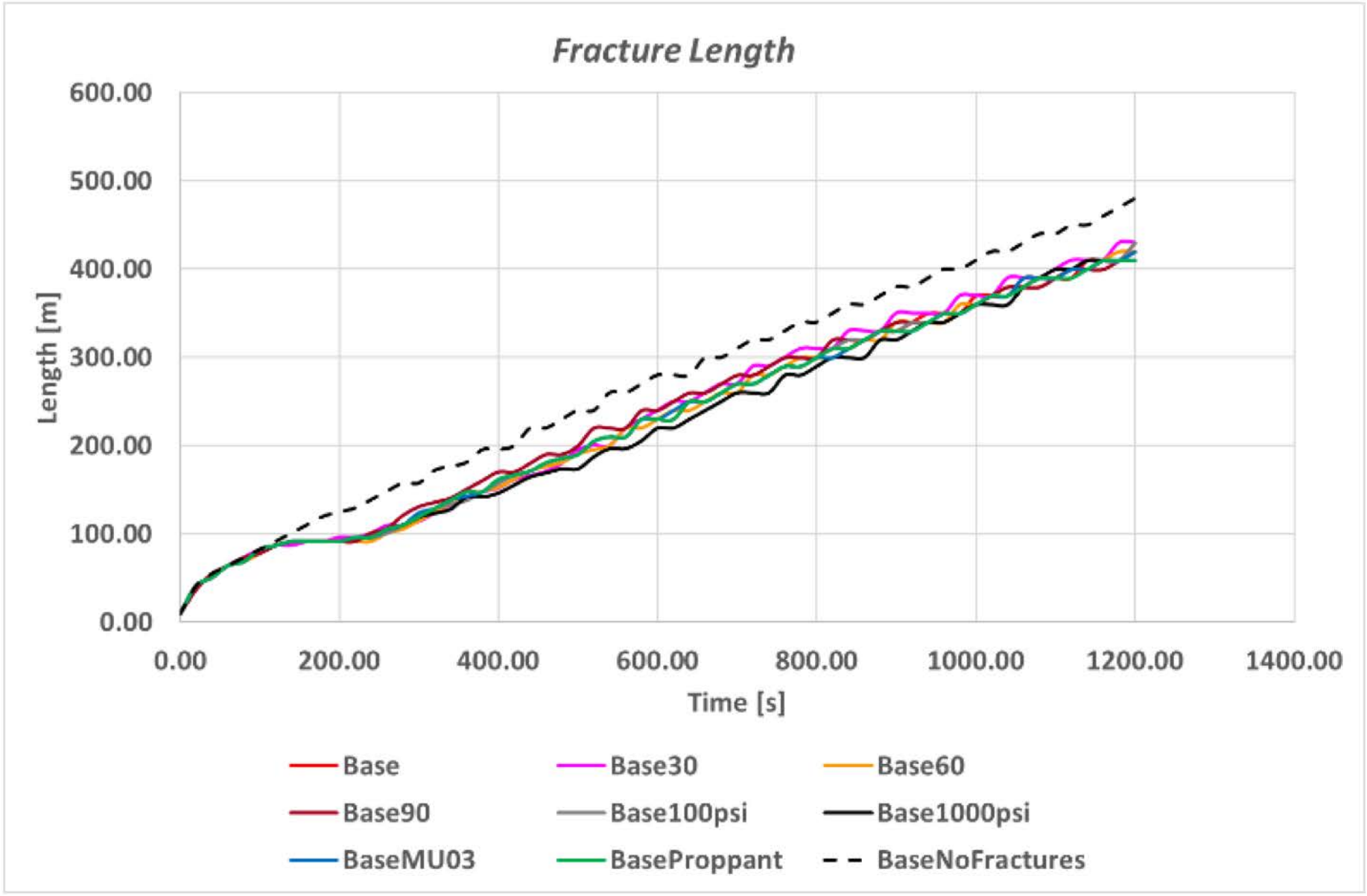

Figure 3. Fracture length measured parallel to the long axis of the fracture (y axis in Figure 1).

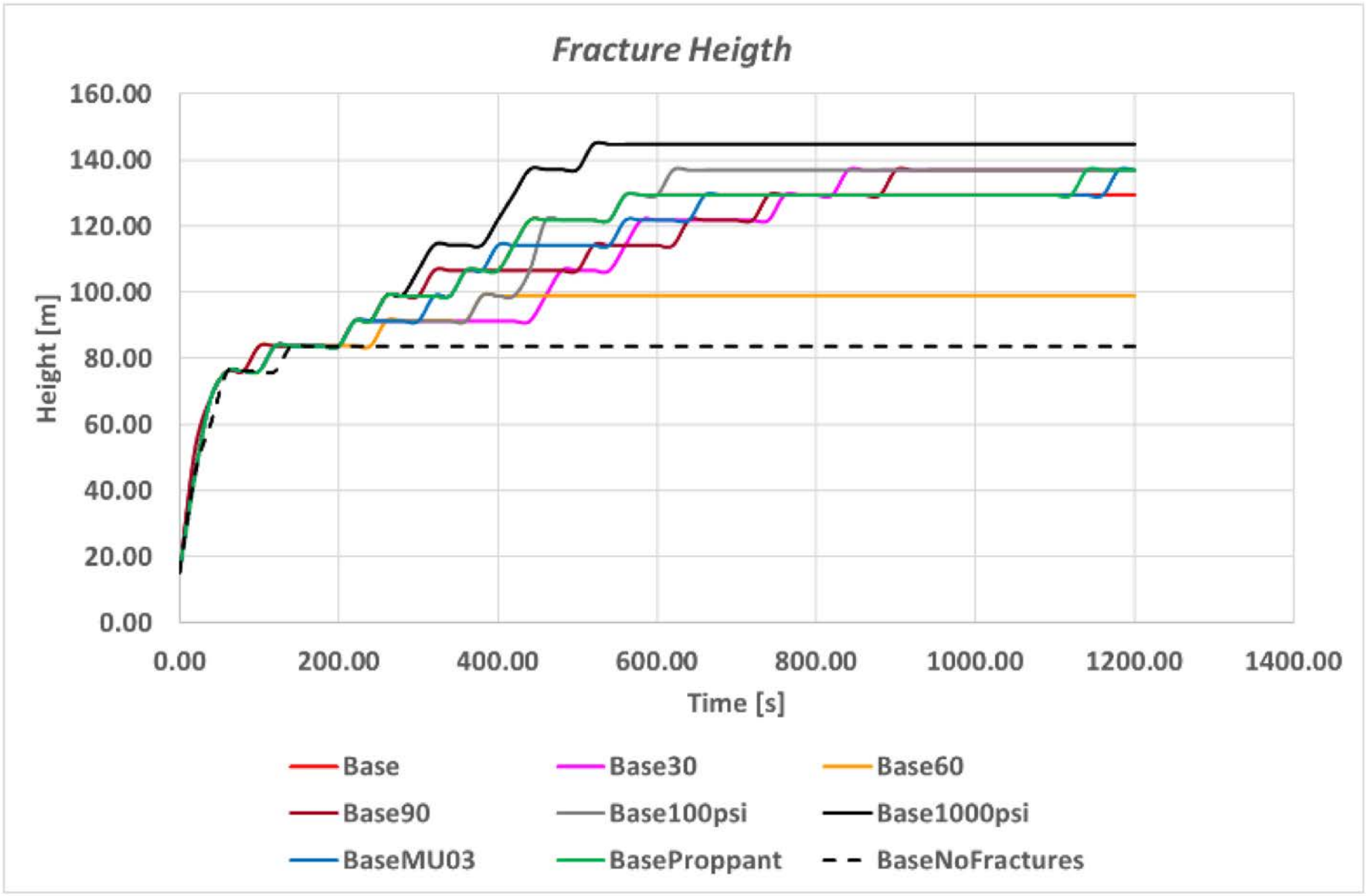

Figure 4. Fracture height measured parallel to the small axis of the fracture (x axis in Figure 1).

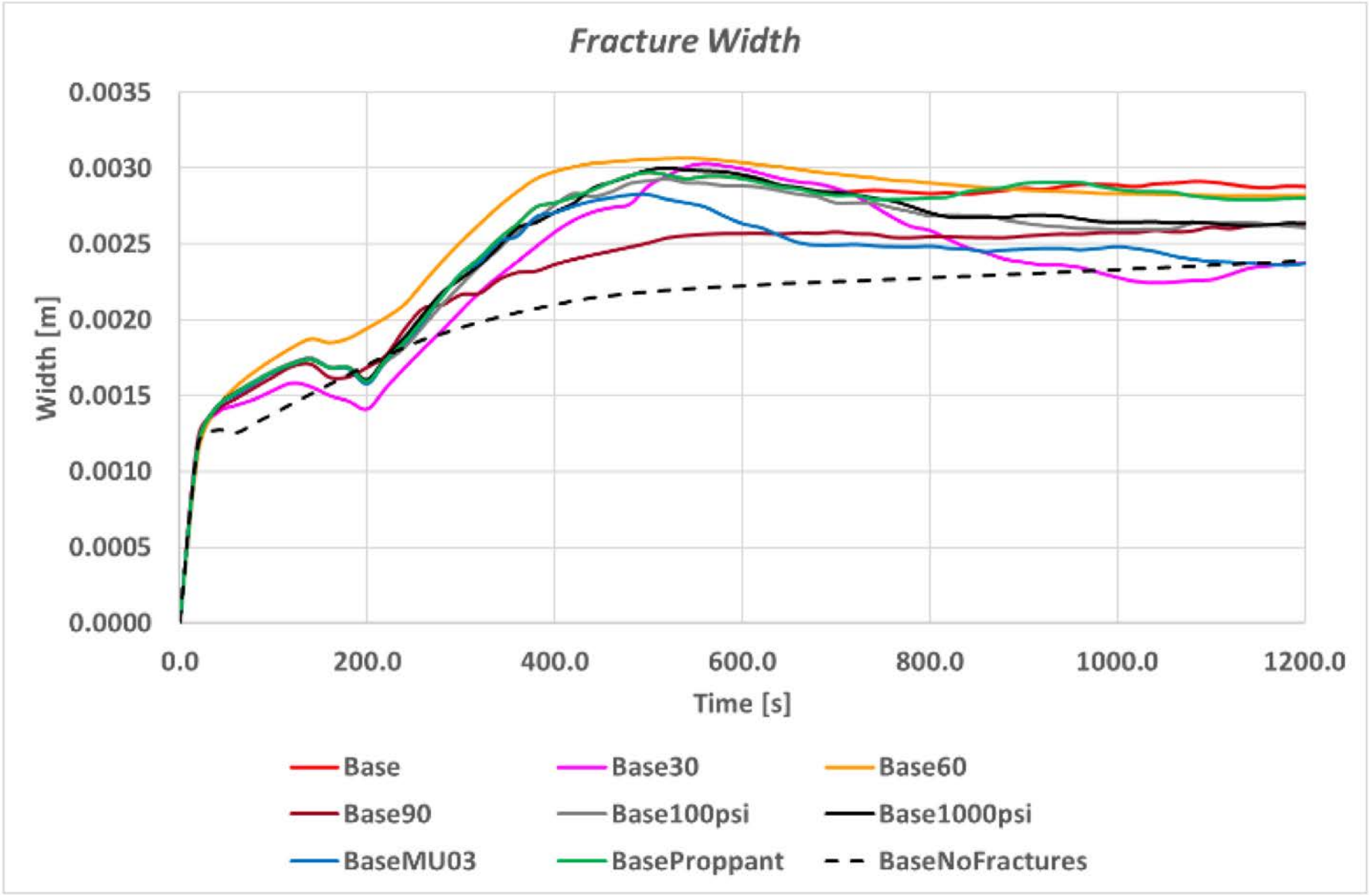

Figure 5. Fracture width measured at the perforation location.

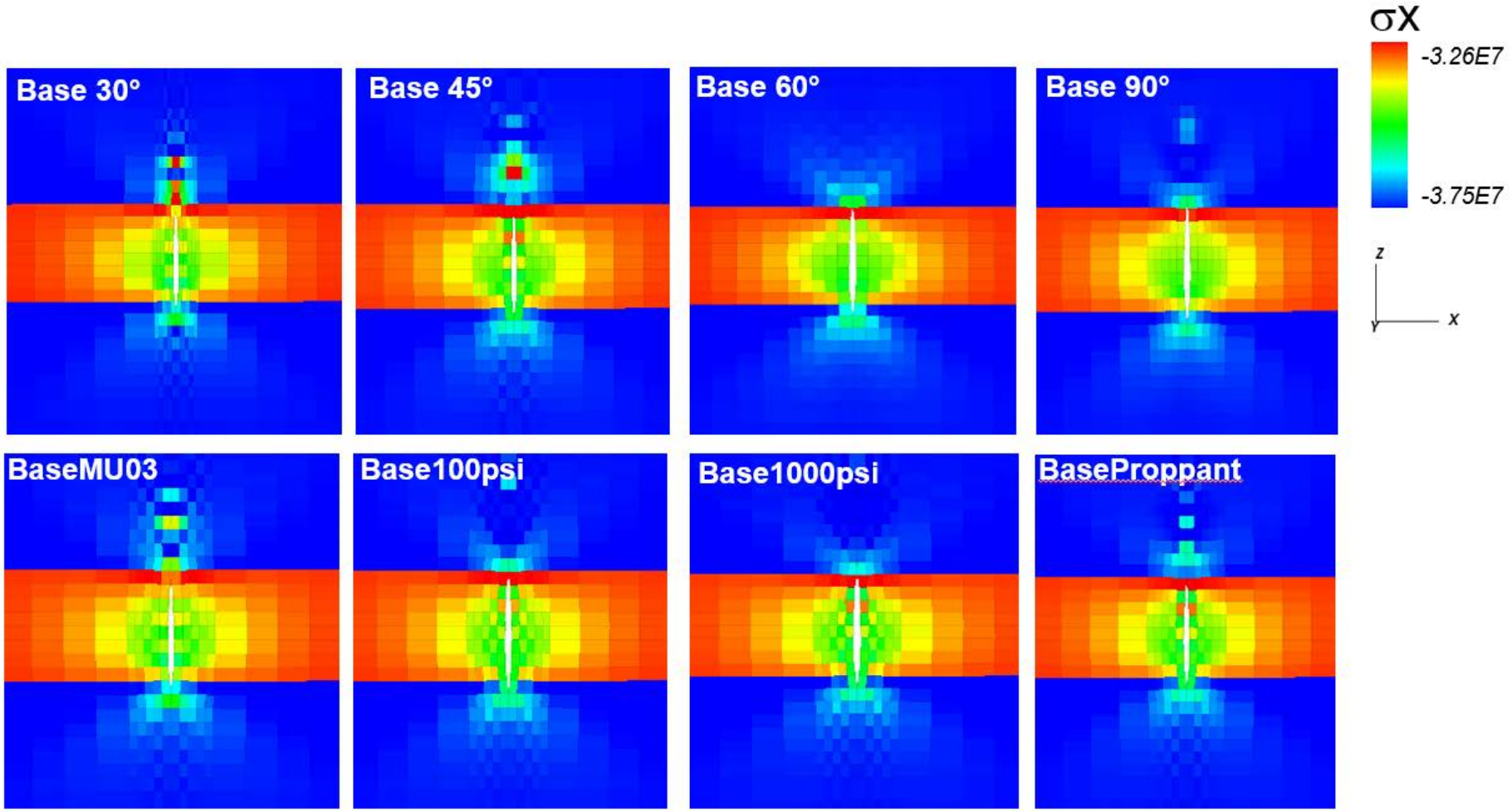

Figure 6. Cross-section view of distribution of Shmin. The section is perpendicular to the hydraulic fracture propagation direction and centered at the perforation. Units in Pa.

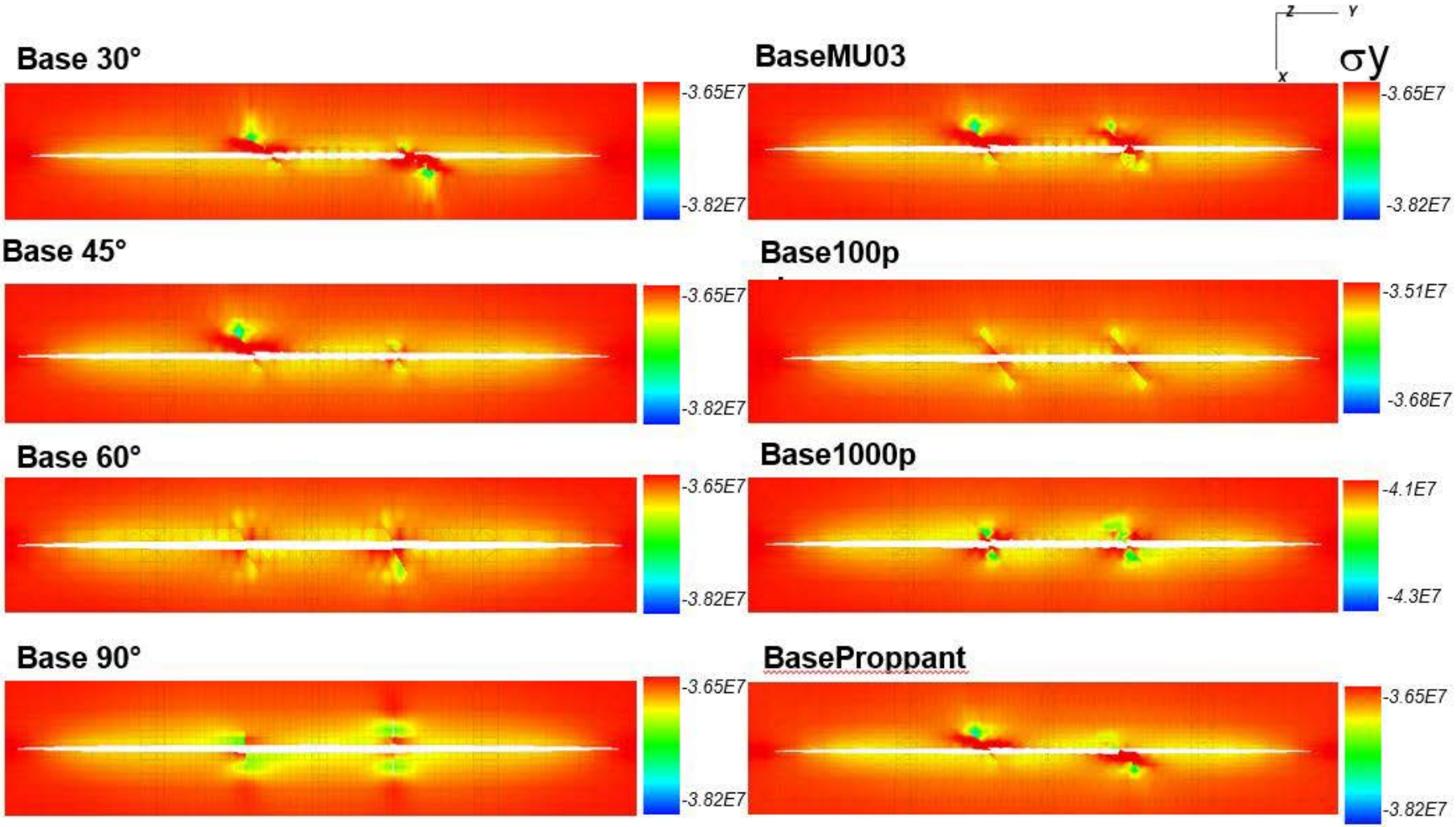

Figure 7. Map view of distribution of SHmax. The section is horizontal and centered at the perforation. Units in Pa.

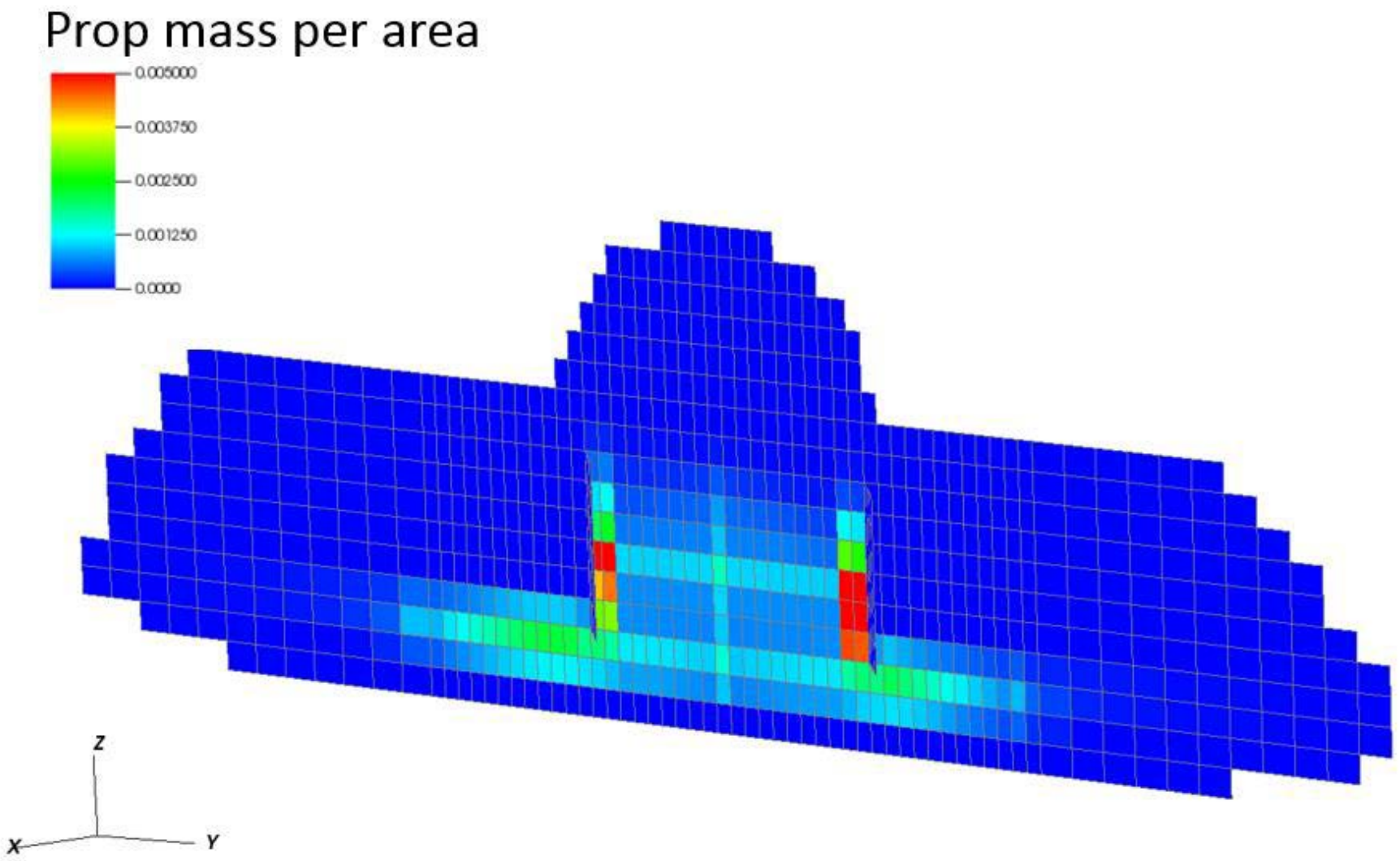

Figure 8. Model including proppant during the stimulation (BaseProppant). Units in kg/m^2.

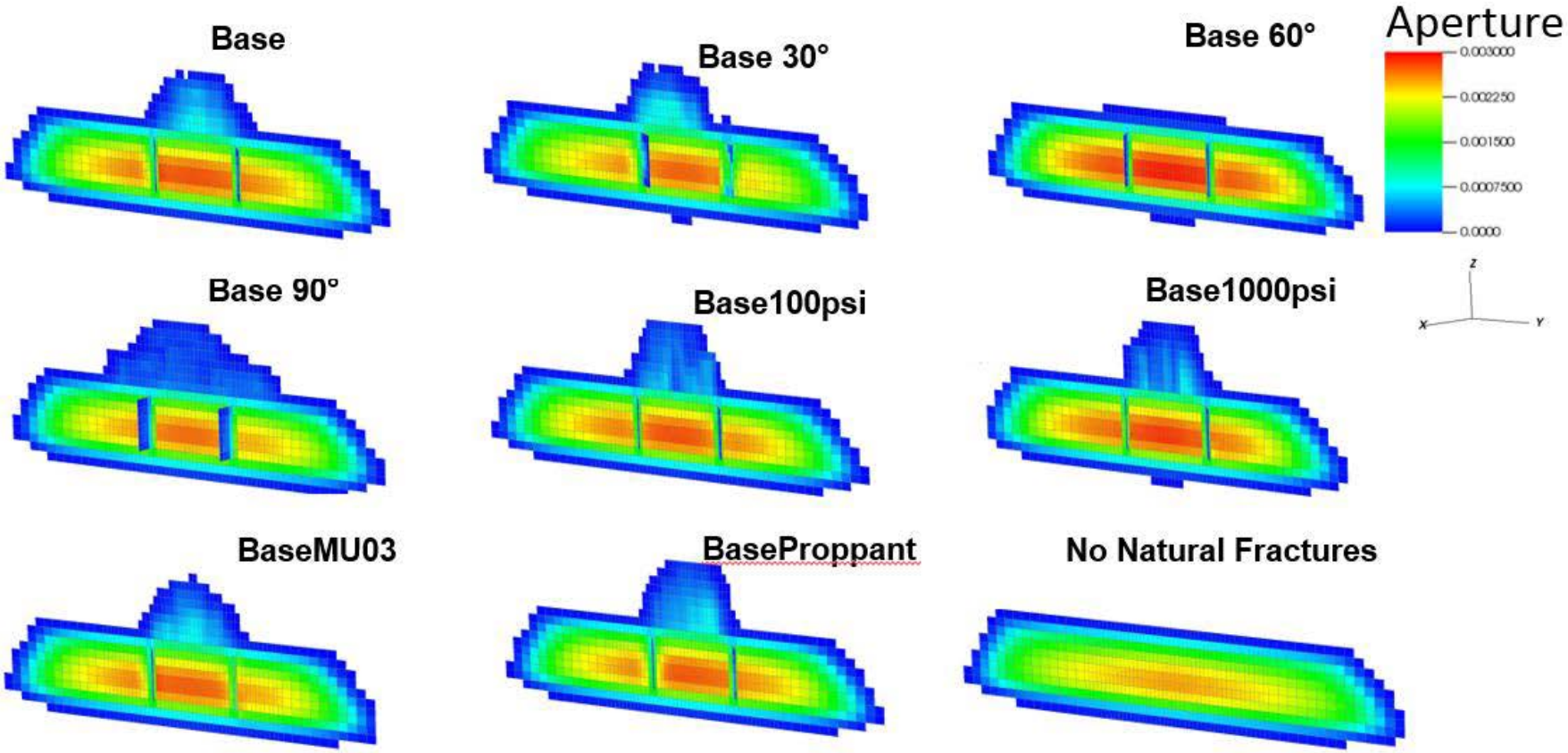

Figure 9. Oblique view of the stimulated fractures colored based on aperture. Units in mm.

Layer	Layer Top	Thickness	Shmin	SHmax	Sv	E	ν	KIc
	[m]	[m]	[Pa]	[Pa]	[Pa]	[GPa]		[Mpa-$m^{0.5}$]
Layer 1	2346.96	60.96	36197490	38265918	48263320	24.13166	0.35	0.549421303
Layer 2	2407.92	60.96	34473800	36542228	48263320	27.57904	0.3	1.098842606
Layer 3	2468.88	60.96	36197490	38265918	48263320	31.02642	0.25	1.648263909

Table 1. Stresses and mechanical properties used in the multilayered stimulation study.

Model Id	Fracture angle	Friction Coefficient	Stress Contrast	Proppant
	[◦]		[psi]	
Base	45	0.6	300	no
Base90	90	0.6	300	no
Base60	60	0.6	300	no
Base30	30	0.6	300	no
BaseMu03	45	0.3	300	no
Base100psi	45	0.6	100	no
Base1000psi	45	0.6	1000	no
BaseProppant	45	0.6	1000	yes
BaseNoFractures	N/A	0.6	300	no

Table 2. Parameters used in the multilayered stimulation study.